Aberrant enhanced NLRP3 inflammasomes and cell pyroptosis in the brains of prion infected rodent models are largely associated with the proliferative astrocytes

Dong-Hua Zhou

  National Institute for Viral Disease Control and Prevention, Chinese Center for Disease Control and Prevention

Xiao-Xi Jia

  National Institute for Viral Disease Control and Prevention, Chinese Center for Disease Control and Prevention

Yue-Zhang Wu

  National Institute for Viral Disease Control and Prevention, Chinese Center for Disease Control and Prevention

Wei-Wei Zhang

  National Institute for Viral Disease Control and Prevention, Chinese Center for Disease Control and Prevention

Yuan Wang

  National Institute for Viral Disease Control and Prevention, Chinese Center for Disease Control and Prevention

Dong-Lin Liang

  National Institute for Viral Disease Control and Prevention, Chinese Center for Disease Control and Prevention

Li-Ping Gao

  National Institute for Viral Disease Control and Prevention, Chinese Center for Disease Control and Prevention

Kang Xiao

  National Institute for Viral Disease Control and Prevention, Chinese Center for Disease Control and Prevention

Cao Chen

  National Institute for Viral Disease Control and Prevention, Chinese Center for Disease Control and Prevention

Xiao-Ping Dong

  National Institute for Viral Disease Control and Prevention, Chinese Center for Disease Control and Prevention

Qi Shi

shiqi@ivdc.chinacdc.cn

National Institute for Viral Disease Control and Prevention, Chinese Center for Disease Control and Prevention

---

Research Article

Additional Declarations: No competing interests reported.

Abstract

Neuroinflammation is a common pathological feature in a number of neurodegenerative diseases, which is mediated primarily by the activated glial cells. NLRP3 inflammasomes associated neuroinflammatory response is mostly considered. To investigate the situation of the NLRP3 related inflammation in prion disease, we assessed the levels of the main components of NLRP3 inflammasome and its downstream biomarkers in the scrapie infected rodent brain tissues. The results showed that the transcriptional and expressional levels of NLRP3, caspase1, ASC in the brains of scrapie infected rodents were significantly increased at terminal stage. The increased NLPR3 overlapped morphologically well with the proliferated GFAP-positive astrocytes, but little with microglia and neurons. Using the brain samples collected at the different time-points after infection, we found the NLRP3 signals increased in a time-dependent manner, which were coincidental with the increase of GFAP. Two main downstream cytokines, IL-1β and IL-18, were also upregulated in the brains of prion infected mice. Moreover, the GSDMD levels, particularly the levels of GSDMD-NT, in the prion infected brain tissues were remarkably increased, indicating activation of cell pyroptosis. The GSDMD not only co-localized well with the astrocytes but also with neurons at terminal stage, also showing a time-dependent increase after infection. Those data indicate that NLRP3 inflammasomes were remarkably activated in the infected brains, which is largely mediated by the proliferated astrocytes. Both astrocytes and neurons probably undergo a pyroptosis process, which may help the astrocytes to release inflammatory factors and contribute to neuron death during prion infection.

Introduction

Prion diseases, also named transmissible spongiform encephalopathies, are a kind of fatal, progressive neurodegenerative diseases which affect humans and various species of mammals. Human prion diseases can be sporadic, inherited or acquired, with a long incubation period and a short disease course[1−3]. The typical neuropathological features of prion diseases include cavernous degeneration, amyloid plaque deposition of PrP^{Sc}, neuron loss and glial cell proliferation[2, 4]. Up to now, there is lacking of specific therapeutic and prophylactic tools for efficiently relieving symptoms or delaying onset.

Glial cells mainly include microglia and astrocytes, which are generally considered to be important neuroimmune cells in the central nervous system (CNS). Neuroinflammation is usually manifested by microglial activation and astrocyte proliferation, accompanied by transcriptome changes, which is a common marker of various neurodegenerative diseases, including prion diseases. Neuroinflammatory responses are mainly induced by a variety of inflammasomes, in which NOD-like receptor thermal protein domain associated protein 3 (NLRP3) is a key regulatory protein[5−7]. NLRP3 inflammasome is a protein complex composed of one NLRP3 containing a PYD domain, one pro-caspase-1 (pro-Cas1) containing a CARD domain, and one apoptosis-associated speck-like protein (ASC) containing both domains mentioned above[5, 8, 9]. Stimulated by pathogen-associated molecular patterns (PAMP) or host-derived damage-associated molecular patterns (DAMP), neuroimmune cells rapidly recruit amounts of pro-Cas1

and ASC that assemble with NLRP3 into inflammasomes via PYD and CARD domains. This process leads to the activation of pro-Cas1 into active caspase-1 (Cas1) that further proteolyzes some pro-inflammatory cytokines (e.g., Il-1β, IL-18) and gasdermin-D (GSDMD)[10–13]. The proteolyzed N-terminal structure (GSDMD-NT) may bind to the acidic phospholipids in the inner lobe of the plasma membrane, punch holes in cell membrane, release the proinflammatory agents, and eventually induce the death of inflammatory cells[14, 15].

NLRP3 inflammasome are described to promote deterioration on the animal models of some neurodegeneration diseases, such as Alzheimer disease (AD), Parkinson disease (PD), Huntington disease (HD), etc.[5, 16, 17]. Knockout of NLRP3 in a transgenic mouse model of AD protects from spatial memory dysfunction and reduces the deposition of Aβ[9, 18]. In the PD mouse model, siRNA-mus-NLRP3 plays a significant neuroprotective role through inhibiting the injury neuron and the proliferation of glial cells[19, 20]. However, the role of NLRP3 inflammasomes in the neuroinflammatory response of prion diseases is unclear.

In the present study, the status of NLRP3 inflammasome in the brain tissues of several prion infected rodent models were comprehensively assessed by different methodologies. The brain levels of NLPR3 in the scrapie infected rodents were increased in a time-dependent manner along with the incubation period. Double-stained immunofluorescent assays identified that the NLPR3 mainly overlapped with the proliferated astrocytes. In parallel, the brain levels of pro-Cas1 and ASC in the scrapie infected rodents were also upregulated. Molecular complexes of NLRP3 with pro-Cas1 and ASC were detected in the brain homogenates. Increases of cytokines Il-1β and IL-18 were also observed in the brains of scrapie infected animals. Furthermore, the brain GSDMD levels of scrapie infected mice upregulated progressively post-infection. These findings illustrate that NLRP3 inflammasomes may play an important role in the neuroinflammation of prion diseases.

Materials and Methods

Ethics Statement

Usage of animal specimens in this study was approved by the Ethical Committee of the National Institute for Viral Disease Prevention and Control, China CDC under protocol 2009ZX10004-101. Animal housing and experimental protocols were in accordance with the Chinese Regulations for the Administration of Affairs Concerning Experimental Animals.

Preparation of brain homogenates

The brain specimens of the experimental rodents infected with various scrapie agents were enrolled, including 263K infected hamsters, 139A- and ME7-infected mice. The animal challenge of intracerebral inoculation was described previously[21-23] and the incubation periods of scrapie agent 263K infected hamsters, as well as 139A- and ME7-infected mice were 66.7±11 days, 183.9±23.1 days and 184.2±11.8 days, respectively. The brain tissues of the age-matched normal hamsters (80 days old) and normal mice

(180 days old) were used as the control. Additionally, the brain tissues of 139A- and ME7-infected mice collected on 80-, 120-, 150-, 180-day post-inoculation (dpi) were recruited into this study, which represented early, middle-early, middle-late, and terminal stage, respectively.

According to the protocol described previously, to prepare the brain homogenates of mice and hamsters, the surgically removed brain samples were homogenized in cold lysis buffer (containing 100 mM NaCl, 0.5 % Nonidet P-40, 0.5 % sodium deoxycholate, 10 mM EDTA and protease inhibitor cocktail set III (Calbiochem)) after weighing (1g/10ml). Crude homogenates were spun shortly, and aliquots of the supernatants were immediately frozen at 80°C for subsequent experiments.

Preparation of paraffin sections of brain tissue

The surgically removed brains of normal and scrapie infected rodents were fixed with 4% paraformaldehyde at 4°C for 16 h, and then moved to an embedding box and rinsed under running tap water for 3 h. The fixed brain tissues were serially dehydrated and soaked in xylene for 1.5 h. The soaked tissue was embedded, and the tissue slices were prepared according to the routine neuropathological protocol.

Western blots

10% of brain homogenates were separated by 12% SDS-PAGE and electronically transferred to nitrocellulose membranes with a Semi-dry facility. After blocking with 5 % nonfat-dried milk in TBS at 37°C for 1 h, the membranes were incubated at 4°C overnight with specific monoclonal or polyclone antibody, including anti-NLRP3 (1:000 dilution, AG-20B-0014-C100, AdipoGen, Switzerland), anti-ASC (1:500 dilution, Santa Cruz, USA) and anti-Caspase1 (1:500 dilution, 06-503-I, Millipore, USA). After washing with TBST (containing 0.1 % Tween-20, pH7.6) for 4 times, the membranes were incubated with horseradish peroxidase-conjugated anti-mouse or anti-rabbit antibody (1:5000 dilution, 115-035-003/111-035-003, Jackson, USA). Immunoreactive signals were developed using an enhanced ECL kit (PE Applied Biosystems, Foster City, CA, USA). Images were captured by ChemiDocTM XRSC Imager (Bio-Rad, USA).

Immunoprecipitation (IP) assay

Magnetic beads were separately incubated with anti-NLRP3, mouse and hamster IgG on a vertical rotating mixer at 4°C for 4 h. After washed with PBST (PBS containing 0.05% Tween 20) for 5 times, various 10% brain homogenates with the total protein content of 100 μg were added and incubated at 4°C overnight on a vertical rotating mixer. The mixtures were washed with PBST for 5 times and the precipitated products were subjected into the Western blots with anti-ASC or anti-pro-Cas1 separately.

Immunofluorescence assay (IFA)

After incubated in the repair buffer (containing 0.4 g citric acid and 3 g trisodium citrate) and heated in microwave oven for 30 min, the brain sections were permeabilized with 0.3% Triton X-100 in PBS for 30

minutes and then blocked with normal goat serum for 1 h. The slices were incubated with different specific antibodies, including 1:100 diluted mouse anti-NLRP3, 1:200 diluted rabbit anti-GFAP (HPA056030, Millipore, USA), 1:200 diluted rabbit anti-NeuN (ab177487, Abcam, Britain) and 1:500 diluted rabbit anti-Iba1 (019-19741, WAKO,) at 4°C overnight. After washing, the sections were incubated with 1:200-diluted Alexa Fluor 488-labeled goat-derived anti-rabbit (A11034, Invitrogen, USA) and Alexa Fluor 568-labeled goat-derived anti-mouse (A11031, Invitrogen, USA) secondary antibodies at 37°C for 1 h, and stained with DAPI (1mg/mL) at room temperature (RT) for 15 min. The slices were sealed and the images were viewed and analyzed using confocal laser microscope system (Leica TCS/SP8, Germany).

Quantitative real-time PCR (qRT-PCR)

Total RNAs from the brain tissues of 139A- and ME7-infected mice collected at end-stage and the age matched health mice were extracted with of the Total RNA Rapid Extraction Kit (R218, GeneBetter, China) according to the instructions of the manufacturer. The first-strand cDNA synthesis was conducted with commercial Script III RT MasterMix kit (P518, GeneBetter, China). The specific primers were designed based on the sequences issued in GenBank and summarized in Table 1. Real-time PCR was performed on a PCR instrument (ABI 7900HT, Applied Biosystems, USA) with the ChamQ Universal SYBR qPCR Master Mix (Q711-02, Vazyme, China). All PCR processes were performed in triplicate with a total of 40 cycles (30 s at 95 °C, 30 s at 60 °C, 60 s at 72 °C). The relative transcriptional level of mRNA was calculated by Ct method ($2^{-\Delta\Delta Ct}$).

Table 1 Information of primers

Primer	Sequence (5' to 3')
mNLRP3-F	TGGAGACACAGGACTCAGGC
mNLRP3-R	CATTTCACCCAACTGTAGGC
mCaspase1-F	TGCCGTGGAGAGAAACAA
mCaspase1-R	ATGAAAAGTGAGCCCCTG
mASC-F	TCAGAGTACAGCCAGAACAGG
mASC-R	CTCCAGGTCCATCACCAAGT
mIL-1β-F	GATACTGCCTGCCTGAAGCTCTTG
mIL-1β-R	TGAAGCAGCTATGGCAACTGTTCC
mIL-18-F	AGTAAGAGGACTGGCTGTGACC
mIL-18-R	TTGGCAAGCAAGAAAGTGTC
mGSDMD-F	TGTCAACCTGTCAATCAAGGA
mGSDMD-R	AGCCAAAACACTCCGGTTC
mGAPDH-F	TTTGCAGTGGCAAAGTGGAG
mGAPDH-R	GATGGGCTTCCCGTTGATGA

ELISA

The brain homogenates were diluted to 500 μg/μl (total protein concentration) with a bicinchoninic acid protein assay kit (71285–3, Novagen, USA). The levels of IL-1β and IL-18 were separately measured with commercial enzyme-linked immunosorbent assay (ELISA) kits (EK0394 for IL-1β, EK0433 for IL-18, Boster, China) according to the manufacturer's instruction.

Statistics

Quantitative analysis of immunoblot images was carried out using software ImageJ. The gray values of each target blot were evaluated. Data shown were means ± SD of triplicate samples from a single experiment and were representative of three independent experiments. Statistical analyses were conducted using Student's t test. *: <0.05; **: <0.01; ***:<0.001.

Results

Increased expression of NLRP3 in the brains of prion infected rodent models at terminal stage

To assess the status of the inflammasome during prion infection, the brain tissues of several prion infected rodents at terminal stage were enrolled into this study. The transcriptional levels of brain NLRP3, one of the components of inflammasome, were evaluated by NLRP3-specifc qRT-PCR. Compared to were 1.5-3 folds increased (Fig. 1A). IFAs with anti-NLRP3 revealed more and larger NLRP3 stained cells in the brain sections of 139A- and ME7-infected mice, as well as that of 263K-infected hamsters, with significantly higher IOD values compared to the individual normal control (Fig. 1B). NLRP3-specifc Western blots identified notably stronger bands in the brain homogenates of 139A- and ME7-infected mice (Fig. 1C), and 263K-infected hamsters (Fig. 1D), with statistical differences in the quantitative assays normalized with the data of the individual normal control. It strongly indicates that the expressions of brain NLRP3 in the prion infected rodent models at final stage are remarkably upregulated.

Morphological colocalization of the increased NLRP3 with the proliferated astrocytes in the brains of prion infected rodents

The brain sections of 139A- and ME7-infected mice and 263K-infected hamsters were subjected into double-stained IFAs with anti-NLRP3 and anti-GFAP, Iba1 or anti-NeuN separately. Confocal images showed obvious morphological overlaps of NLRP3 (*red*) with GFAP (*green*) signals in the background of amounts of large astrocytes both in the regions of cortex and hippocampus of 139A- and ME7-mice (Fig. 2A, left panel), and those of 263K-infected hamsters (2B, left panel). NLRP3 stained asteroid cells (*red*) distributed around the Iba1 (middle panel) and NeuN (right panel) stained cells (*green*), however, did not overlap each other in the brain sections of normal and infected animals. It implies the increased NLRP3 in the prion infected experimental rodents mainly distributes in the proliferated astrocytes.

Increased expression of Cas1 and ACS in the brains of prion infected rodent models at terminal stage

The expressions of Cas1 and ACS, the other two components of inflammasome, in the brain tissues of prion infected rodents were also evaluated. Remarkably upregulated Cas1 transcriptions in the brains of 139A- and ME7-infected mice were found by Cas-l-specific qRT-PCR (Fig. 3A). Similarly, ACS-specific qRT-PCR assays also revealed an increased transcription of ACS in the brains of both 139A- and ME7-infected mice compared to that of normal control (Fig. 3B). IFAs with anti-Cas1 showed more green signals in the brain sections of 139A- and ME7-infected mice and 263K-infected hamsters, with statistical difference to that of normal control (Fig. 3C).

The brain sections were further employed to double-stained IFAs with anti-NLRP3 and anti-Cas1. Differing to the large asteroid-like cells stained by anti-NLRP3 (*red*), the Cas1-specific signals were small graininess (*green*) widely distributing in the brain tissues (cortex and hippocampus) of three scrapie infected rodent models (Fig. 3D). Amounts of yellow signals were identifiable in the merged images, highlighting colocalizations between NLRP3 and Cas1 morphologically. Further, the molecular interaction of NLRP3 with Cas1 and ACS in brain tissues were estimated by IP assays. Same amounts of 10% brain homogenates of 139A- and ME7-infected mice, as well as that of 263K-infected hamsters, were separately immunoprecipitated with anti-NLRP3 controlled by the brain homogenates of individual

normal control. In the blots with anti-Cas1 (Fig. 3E), specific Cas1 bands were detected in the elution fractions but not in that precipitated by isotype IgG. Quantitative assays verified significantly higher relative gray values in prion infected mice (upper panel) and hamsters (low panel) compared to the control. Specific ACS bands were also identified in the IP assays of both mouse and hamster brain homogenates, using anti-NLRP3 as capturing antibody and anti-ACS as detecting antibody (Fig. 3F). Markedly stronger ACS bands were observed in the preparations of prion infected mice and hamsters, showing statistical differences compared to the controls in the quantitative assays. Those date indicate that the expressions of Cas1 and ACS also increase in the brains of prion infected rodents. NLRP3 can form protein complexes with Cas1 and ACS in brain tissues.

Time-dependent increases of brain NLRP3 levels during prion infection

To estimate the alteration of brain NLRP3 during prion infection, the brain sections of 139A- and ME7-infected mice collected on 80, 120, 150 and 180 dpi were immunofluorescently stained by anti-NLPR3 and anti-GFAP separately. As shown in Fig. 4, notably more GFAP-stained astrocytes (*green*) were detectable in the slices of 80 dpi and continually increased in the subsequent slices of both 139A- (left) and ME7- (right) infected mice. NLRP3 signals (*red*) also increased gradually along with the sampling time. Further assays of the fluorescent intensities proposed that time-dependent increases of both brain GFAP and NLPR3 during the incubation of prion infection. Compared to the data of normal mice with the age of 180 days, GFAP-stained cells became significant since 80 dpi both in cortex and hippocampus regions, while NLRP3 signals were significantly upregulated since 120 dpi, particularly in the region of cortex. It highlights a time-dependent increase of brain NLPR3 during prion infection, which is coincidental with the increase of proliferative astrocytes.

Increased Il-1β and IL-18 levels in the brains of prion infected rodent models at terminal stage

As one of the important downstream components of inflammasome, the brain levels of Il-1β and IL-18 in the prion infected rodents at terminal stage were evaluated. qRT-PCR assays of the extracted brain RNAs found that the brain Il-1β and IL-18 transcriptional levels in 139A- and ME7-infected mice were significantly higher than those of normal mice (Fig. 5A). Subsequently, the Il-1β and IL-18 levels in the brains of various experimental rodents were measured by a commercial kit. Compared to the individual control, the brain Il-1β levels of two prion infected mice models and the hamster model were significantly increased, while IL-18 levels of prion infected mice significantly upregulated and that of prion infected increased but without statistical difference (Fig. 5B). Il-1β-specific IFAs revealed more green particles in the regions of cortex and hippocampus of 139A- and ME7-infected mice and 263K-infected hamsters, which distributed widely in the brains, and some of them overlapped with the NLRP3-stained asteroid-like cells (*red*) (Fig. 5C).

Increased GSDMD levels in the brains of prion infected rodent models

Gasdermin D (GSDMD) is the biomarker for pyroptosis, which is hydrolyzed and activated by Cas1. To assess the status of GSDMD in the brain tissues during prion infected, the brain specimens of 139A infected mice at terminal stage were evaluated. qRT-PCR assays identified significantly increased mRNA level of GSDMD in the brains of 139A infected mice (Fig. 6A). Western blots revealed stronger GSDMD-NT specific bands in the brains of 139A-infected mice with statistical significance compared to that of normal mice in the quantitative assay (Fig. 6B). IFAs illustrated remarkably more and larger GSDMD-specific signals (*green*) in the brain regions (cortex and hippocampus) of 139A-infected mice, showing significantly higher IOD values compared to those of normal control (Fig. 6C).

Subsequently, the brain sections of 139A-infected mice collected on 120-, 150-, and 180- (terminal stage) dpi were subjected into double-stained IFAs with anti-GSDMD and anti-NLRP3. Accompanying with the increases of NLRP3 signals (*red*), the intensities of GSDMD signals (*green*) in the cortex and hippocampus of prion infected mice increased gradually along with the incubation period (Fig. 6D). Analysis of the enlarged images identified that the GSDMD signals distributed not only in the asteroid-like cells that colocalized well with NLRP3 signals (*yellow* in the merged images), but also in the round and elliptical cells that overlapped little with NLRP3 signals. To estimate the distribution of the increased GSDMD in the different cell types in the prion infected brains, the brain slices of 139A-infected mice at terminal stage were subjected into double stained IFAs of anti-GSDMD together with anti-GFAP, anti-NeuN or anti-Iba1. GSDMD signals overlapped with GFAP- and NeuN-positive cells, but not with Iba1-positive cells (Fig. 6E). Those data strongly indicate a time-dependent increase of brain GSDMD during prion infection, which distributes widely in astrocytes and neurons at the end of disease.

Discussion

Inflammasomes are a class of multiprotein complexes assembled with the participation of intracytoplasmic pattern recognition receptors (PRRs), which are important components of natural immune system. A variety of inflammasomes, such as NLRP1- NLRP3-, NLRC4-, IPAF- and AIM2-inflammasomes, have been described to be involved in host responses against a wide range of pathogens [10, 24, 25]. By mediating neuroinflammation, NLRP3 inflammasomes are considered to play a vital role in the progressions of some neurodegenerative diseases. For example, Aβ can activate NLRP3 inflammasomes in glial cells, which further promotes the formation of ASC spots, maturation and release of IL-1β, and accelerate memory loss and other symptoms in AD mouse models[9]. In a PD mouse model, stimulation of mitochondrial autophagy or acceleration of removing damaged mitochondria inhibit the activation of NLRP3 inflammasomes in microglia, which remits the loss of dopaminergic neurons and ameliorates the clinical symptoms[19]. Activation of NLRP3 inflammasomes have also reported in other neurodegenerative disorders, e.g., amyotrophic lateral sclerosis (ALS) and multiple sclerosis[26, 27]. Here, using the brain samples of several prion infected rodent models, we have verified overexpression of NLRP3 inflammatory vesicle components with time-dependent manner after inoculation. Coincidentally, the brain levels of the downstream inflammatory cytokines IL-1β and IL-18, and the membrane perforating protein GSDMD-NT are significantly increased, which may promote the release of inflammatory factors during prion infection. Our data here demonstrate again the similar

response of brain NLRP3 inflammasomes of prion diseases as other neurodegenerative diseases, although their etiological, neuropathological, clinical features are different.

Astrocytes in CNS play an important physiological role in providing energy and nutrients to neurons, regulating synaptic activity, and regulating extracellular glutamate levels. On the other hand, astrocytes may produce toxic effects on neighbor neurons by releasing inflammatory factors during the pathogenic courses of neurodegenerative diseases[28, 29]. Our IFAs in this study demonstrate an overwhelming morphological overlap of NLRP3 with astrocytes but not with microglia and neurons in the prion infected experimental rodents, which highly indicates that the over-proliferative astrocytes are likely to be responsible for the enhanced brain NLRP3 inflammasomes during prion infection. In many AD and PD mice models, overexpression of NLRP3 is identified mainly associated with the activated microglia[5, 9], and a few studies demonstrate NLRP3 inflammasomes in astrocytes[5, 29, 30]. Several *in vitro* studies also figure out overexpression of NLRP3 inflammasomes in microglia after stimulation of PrP106-126 peptide[31, 32]. Notably, microglia are the main source for NLRP3 inflammasomes in AD and PD mice models. The exact reason why NLRP3 expression confines in astrocytes in this study is unknown. Certainly, we could not exclude the technical reasons, e.g., the NLRP3 antibody used in this study. However, our IFAs for GSDMD also illustrate similar pattern as NLRP3, that GSDMD signals overlap well with astrocytes but little with microglia. Recent studies on AD and PD have showed that the classical astrocyte-mediated neuroinflammatory response is dependent on the induction of microglia activation[5, 33]. Further comparative analysis the activation of NLRP3 inflammasomes in AD, PD and PrD, regardless of patients' brains or animal models is deserved for address the potential difference among those neurodegenerative diseases.

NLRP3 inflammasome consists of three components, NLRP3, ASC and Cas1. Upon activation, these three components undergo conformational change to assemble and form the NLRP3 inflammasomes[34, 35]. In line with the increase of brain NLRP3 in the prion infected rodents, the overall transcriptional and expressional levels of ASC and caspase-1 are also upregulated. Importantly, our data here also demonstrate the direct molecular interaction of NLRP3 with ASC and Cas1 in the brain tissues, and the markedly more of NLRP3-ASC and NLRP3-Cas1 complexes in the prion infected brains. Coincidentally, the elevated brain levels of IL-1β and IL-18, the main downstream targets of NLRP3 inflammasomes, are also detected in prion-infected mice. Apparently, infection of prion agents sufficiently induces increases of expression, assembly and activity of NLRP3 inflammasomes in the brain tissues.

Another positive evidence for activation of NLRP3 inflammasomes during prion infection is the aberrant upregulation of GSDMD, particularly GSDMD-NT, in brain tissues. It is well known that the activated gasdermin proteins is closely related with cellular pyroptosis, also known as cellular inflammatory necrosis. This process relies on the activation of the caspases IL-1β and IL-18 by the inflammasomes. The active caspases further cleave GSDMD, and the cleaved GSDMD-NT translocate to the cell membrane and form pores, ultimately leading to cytoplasmic efflux, the release of inflammatory factors and cell rupture[14, 36]. The well morphological colocalizations of the increased GSDMD signals with

NLRP3- and GFAP-positive cells in the brains of prion infected mice suggest that cell pyroptosis occurs aggravatedly in the proliferated astrocytes, which is dependent on activation of inflammasomes. One may speculate that the pyrotostic process in astrocytes helps the cells to release inflammatory factors that participate in the neuroinflammation during prion infection. Unlike the distribution of NLRP3, GSDMD signals here are also detectable in the neurons of prion infected mice, particularly in the region of hippocampus at terminal stage. Neuron loss is one of neuropathological features for prion diseases[37, 38] and our previous studies using Nissl stain has demonstrated severe neuron loss in those prion infected rodent models at final stage[39]. As cell pyroptosis is one of the pathways for programmed cell death pathophysiologically, one may assume the possibility that the pyroptosis contributes, at least partially, to the neuron death in prion infection, although the mechanism of cross-talking of NLRP3-inflammasomes between astrocytes and neurons is unclear.

Our data here also present a time-related increase of brain GFAP-NLRP3-GSDMD in the incubation period of prion infection, in which increase of GFAP appears apparently earlier. It highlights a time-dependent correlation among the astrogliosis, NLRP3-inflammasomes, and cell pyroptosis in the brains of prion infection. Aggregations of the misfolding proteins in neurodegenerative diseases are able to trigger the NLRP3 associated neuroinflammatory responses[40, 41]. Certain cellular pathologies, e.g., dysfunction of autophagy, ROS production, mitochondrial injury, lysosomal damage, etc., are also responsible for the activation of NLRP3 inflammasomes[42, 43]. The accumulation of PrP^{Sc} and above cellular pathologies worsen gradually during prion disease. Thereby, it is supposable that the activation of NLRP3 inflammasomes during prion infection is a combined outcome mediated by multiple pathological elements. Given the gradual enhancement and persistent presence of NLRP3 inflammasomes signature in a number of neurodegenerative diseases, including prion disease, the development of NLRP3 inhibitors has been becoming a therapeutic approach to delay the disease progression[17, 29, 44, 45]. However, considering the markedly short duration of prion disease after onset, there will be more challenges in the R&D of therapeutic tools, including NLRP3 modulator, for such rare but fatal disease.

Declarations

Ethics Approval Not applicable.

Consentto Participate Not applicable.

Consentfor Publication Not applicable.

Availability of data and materials Not applicable.

References

1. Ma, Y., et al., *Stimulations of the Culture Medium of Activated Microglia and TNF-Alpha on a Scrapie-Infected Cell Line Decrease the Cell Viability and Induce Marked Necroptosis That Also Occurs in the Brains from the Patients of Human Prion Diseases.* ACS Chem Neurosci, 2019. **10**(3): p. 1273-1283.

2. Zhou, D.H., et al., *Stilbene Compounds Inhibit the Replications of Various Strains of Prions in the Levels of Cell Culture, PMCA, and RT-QuIC Possibly via Molecular Binding.* ACS Chem Neurosci, 2020. **11**(14): p. 2117-2128.

3. Mead, S., et al., *Prion protein monoclonal antibody (PRN100) therapy for Creutzfeldt-Jakob disease: evaluation of a first-in-human treatment programme.* Lancet Neurol, 2022. **21**(4): p. 342-354.

4. Ma, Y., et al., *Reduction of NF-κB (p65) in Scrapie-Infected Cultured Cells and in the Brains of Scrapie-Infected Rodents.* ACS Chem Neurosci, 2017. **8**(11): p. 2535-2548.

5. Heneka, M.T., R.M. McManus, and E. Latz, *Inflammasome signalling in brain function and neurodegenerative disease.* Nat Rev Neurosci, 2018. **19**(10): p. 610-621.

6. Moonen, S., et al., *Pyroptosis in Alzheimer's disease: cell type-specific activation in microglia, astrocytes and neurons.* Acta Neuropathol, 2023. **145**(2): p. 175-195.

7. Ising, C., et al., *NLRP3 inflammasome activation drives tau pathology.* Nature, 2019. **575**(7784): p. 669-673.

8. Zhang, Y., et al., *Gut microbiota from NLRP3-deficient mice ameliorates depressive-like behaviors by regulating astrocyte dysfunction via circHIPK2.* Microbiome, 2019. **7**(1): p. 116.

9. Heneka, M.T., et al., *NLRP3 is activated in Alzheimer's disease and contributes to pathology in APP/PS1 mice.* Nature, 2013. **493**(7434): p. 674-8.

10. Barnett, K.C., et al., *A 360° view of the inflammasome: Mechanisms of activation, cell death, and diseases.* Cell, 2023. **186**(11): p. 2288-2312.

11. Nozaki, K., et al., *Caspase-7 activates ASM to repair gasdermin and perforin pores.* Nature, 2022. **606**(7916): p. 960-967.

12. Knorr, M., et al., *Effect of PDGF-AB heterodimer on a corneal epithelial cell line.* Eur J Cell Biol, 1992. **57**(2): p. 202-9.

13. Ma, X., et al., *Prussian Blue Nanozyme as a Pyroptosis Inhibitor Alleviates Neurodegeneration.* Adv Mater, 2022. **34**(15): p. e2106723.

14. Liu, X., et al., *Inflammasome-activated gasdermin D causes pyroptosis by forming membrane pores.* Nature, 2016. **535**(7610): p. 153-8.

15. Wang, X., et al., *PCSK9 regulates pyroptosis via mtDNA damage in chronic myocardial ischemia.* Basic Res Cardiol, 2020. **115**(6): p. 66.

16. Siew, J.J., et al., *Galectin-3 is required for the microglia-mediated brain inflammation in a model of Huntington's disease.* Nat Commun, 2019. **10**(1): p. 3473.

17. Wu, A.G., et al., *Targeting microglial autophagic degradation in NLRP3 inflammasome-mediated neurodegenerative diseases.* Ageing Res Rev, 2021. **65**: p. 101202.

18. Xu, F., et al., *Engineered Extracellular Vesicles with SHP2 High Expression Promote Mitophagy for Alzheimer's Disease Treatment.* Adv Mater, 2022. **34**(49): p. e2207107.

19. Panicker, N., et al., *Neuronal NLRP3 is a parkin substrate that drives neurodegeneration in Parkinson's disease.* Neuron, 2022. **110**(15): p. 2422-2437.e9.

20. Lawrence, G., C.L. Holley, and K. Schroder, *Parkinson's disease: connecting mitochondria to inflammasomes.* Trends Immunol, 2022. **43**(11): p. 877-885.

21. Xiao, K., et al., *Re-infection of the prion from the scrapie-infected cell line SMB-S15 in three strains of mice, CD1, C57BL/6 and Balb/c.* Int J Mol Med, 2016. **37**(3): p. 716-26.

22. Kim, Y.S., et al., *Incubation periods and survival times for mice injected stereotaxically with three scrapie strains in different brain regions.* J Gen Virol, 1987. **68 (Pt 3)**: p. 695-702.

23. Shi, Q., et al., *Mouse-adapted scrapie strains 139A and ME7 overcome species barrier to induce experimental scrapie in hamsters and changed their pathogenic features.* Virol J, 2012. **9**: p. 63.

24. Chou, W.C., et al., *The NLR gene family: from discovery to present day.* Nat Rev Immunol, 2023. **23**(10): p. 635-654.

25. Kibby, E.M., et al., *Bacterial NLR-related proteins protect against phage.* Cell, 2023. **186**(11): p. 2410-2424.e18.

26. Singh, J., M.L. Habean, and N. Panicker, *Inflammasome assembly in neurodegenerative diseases.* Trends Neurosci, 2023. **46**(10): p. 814-831.

27. Shao, S., et al., *Therapeutic potential of the target on NLRP3 inflammasome in multiple sclerosis.* Pharmacol Ther, 2021. **227**: p. 107880.

28. Osso, L.A. and J.R. Chan, *Astrocytes Underlie Neuroinflammatory Memory Impairment.* Cell, 2015. **163**(7): p. 1574-6.

29. Zhu, J., et al., *Dopamine D2 receptor restricts astrocytic NLRP3 inflammasome activation via enhancing the interaction of β-arrestin2 and NLRP3.* Cell Death Differ, 2018. **25**(11): p. 2037-2049.

30. Giordano, A.M.S., et al., *DNA damage contributes to neurotoxic inflammation in Aicardi-Goutières syndrome astrocytes.* J Exp Med, 2022. **219**(4).

31. Shi, F., et al., *The NALP3 inflammasome is involved in neurotoxic prion peptide-induced microglial activation.* J Neuroinflammation, 2012. **9**: p. 73.

32. Lai, M., et al., *The NLRP3-Caspase 1 Inflammasome Negatively Regulates Autophagy via TLR4-TRIF in Prion Peptide-Infected Microglia.* Front Aging Neurosci, 2018. **10**: p. 116.

33. Li, S., et al., *Microglial NLRP3 inflammasome activates neurotoxic astrocytes in depression-like mice.* Cell Rep, 2022. **41**(4): p. 111532.

34. Niu, T., et al., *NLRP3 phosphorylation in its LRR domain critically regulates inflammasome assembly.* Nat Commun, 2021. **12**(1): p. 5862.

35. Hochheiser, I.V., et al., *Structure of the NLRP3 decamer bound to the cytokine release inhibitor CRID3.* Nature, 2022. **604**(7904): p. 184-189.

36. Wang, C., et al., *NLRP3 inflammasome activation triggers gasdermin D-independent inflammation.* Sci Immunol, 2021. **6**(64): p. eabj3859.

37. Wang, J., et al., *Treatment of SMB-S15 Cells with Resveratrol Efficiently Removes the PrP(Sc) Accumulation In Vitro and Prion Infectivity In Vivo.* Mol Neurobiol, 2016. **53**(8): p. 5367-76.

38. Sigurdson, C.J., J.C. Bartz, and M. Glatzel, *Cellular and Molecular Mechanisms of Prion Disease.* Annu Rev Pathol, 2019. **14**: p. 497-516.

39. Xu, Y., et al., *Activation of the macroautophagic system in scrapie-infected experimental animals and human genetic prion diseases.* Autophagy, 2012. **8**(11): p. 1604-20.

40. Trudler, D., et al., *Soluble α-synuclein-antibody complexes activate the NLRP3 inflammasome in hiPSC-derived microglia.* Proc Natl Acad Sci U S A, 2021. **118**(15).

41. Yang, T., et al., *Concurrent suppression of Aβ aggregation and NLRP3 inflammasome activation for treating Alzheimer's disease.* Chem Sci, 2022. **13**(10): p. 2971-2980.

42. Su, L., et al., *Mitochondria ROS and mitophagy in acute kidney injury.* Autophagy, 2023. **19**(2): p. 401-414.

43. Zhu, M., et al., *Cell-Penetrating Nanoparticles Activate the Inflammasome to Enhance Antibody Production by Targeting Microtubule-Associated Protein 1-Light Chain 3 for Degradation.* ACS Nano, 2020. **14**(3): p. 3703-3717.

44. Harrison, D., et al., *Discovery of Clinical Candidate NT-0796, a Brain-Penetrant and Highly Potent NLRP3 Inflammasome Inhibitor for Neuroinflammatory Disorders.* J Med Chem, 2023.

45. Coll, R.C., et al., *A small-molecule inhibitor of the NLRP3 inflammasome for the treatment of inflammatory diseases.* Nat Med, 2015. **21**(3): p. 248-55.
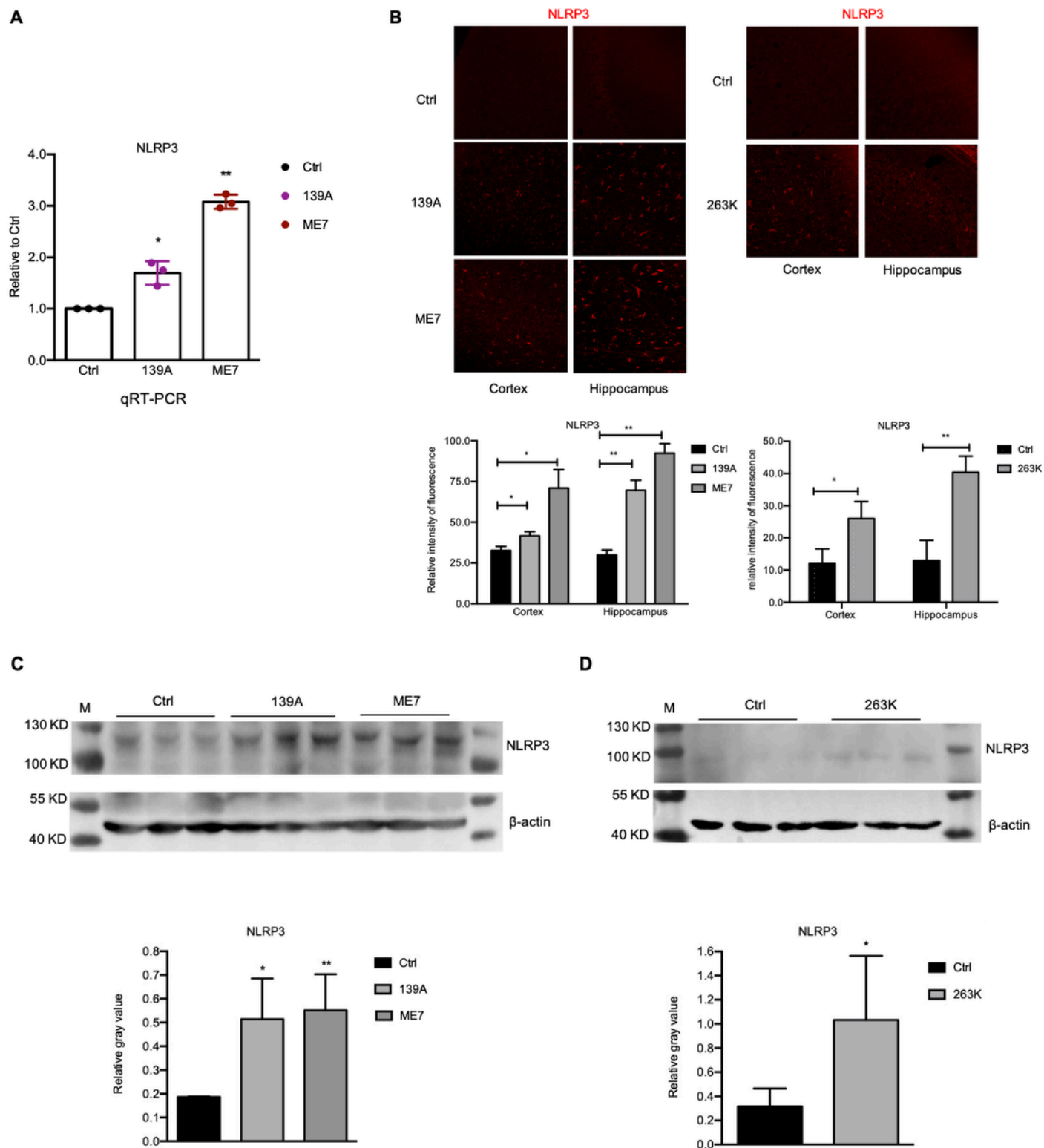
Figures

Figure 1

Analyses of brain NLRP3 in the prion infected rodent models at terminal stage. **A.** NLRP3 specific qRT-PCR of the brain RNAs of scrapie agents 139A- or ME7-infected mice and the age-matched mice. Relative fold changes of NLRP3 mRNAs are marked on Y-axis. Graphical data denote mean + SD (n=3). **B.** Representative images of NLRP3 specific IFAs of the brain sections of scrapie agents 139A- and ME7-infected mice (*left*) and 263K-infected hamsters (*right*). Relative fluorescent intensities of NLRP3 signals

(*red*) in the brain slices of prion infected animals compared to the individual controls (n=3) are showed on the bottom. **C.** NLRP3 specific Western blots of the brain homogenates of 139A- and ME7-infected mice. **D.** NLRP3 specific Western blots of the brain homogenates of 263K-infected hamsters. The relative gray values of NLRP3 normalized with the individual β-actin (n=3) are marked below each panel.
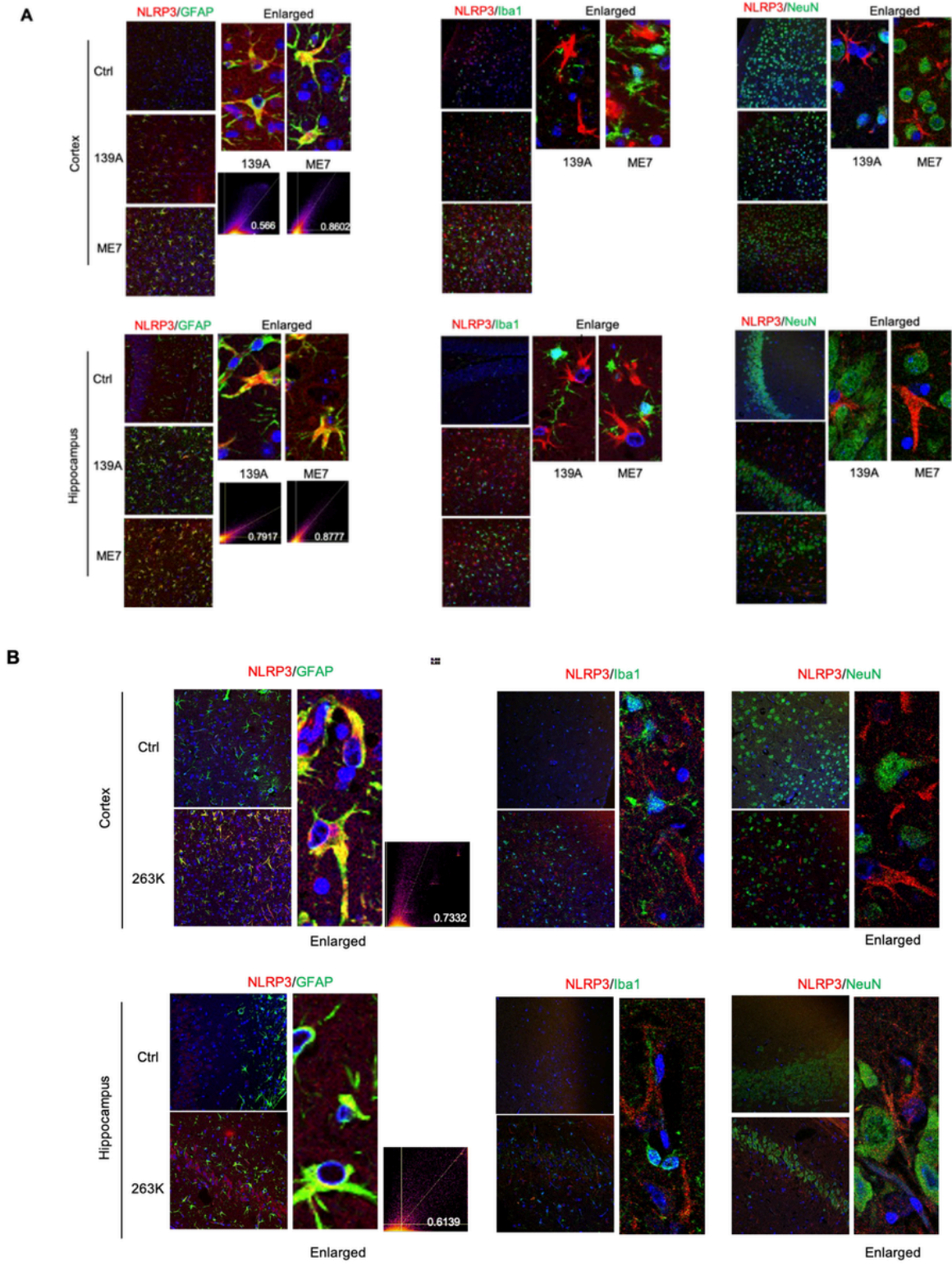

Figure 2

Double stained IFAs for morphological colocalization of NLRP3 with various biomarkers in the brain sections of the prion infected rodent models at terminal stage. **A.** Representative merged images of NLRP3 (*red*) with GFAP (*green, left*), NeuN (*green, middle*) or Iba1(*green, right*) in the brain slices of 139A- and ME7-infected mice. **B.** Representative merged images of NLRP3 (*red*) with GFAP (*green, left*), Iba1(*green, middle*) or NeuN (*green, right*) in the brain slices of 263K-infected hamsters. Brain regions of cortex and hippocampus are indicated on the left. The enlarged images of prion infected animals are showed on the right each graph. Pearson's correlation coefficient test results of NLRP3 and GFAP are marked below or on the right.
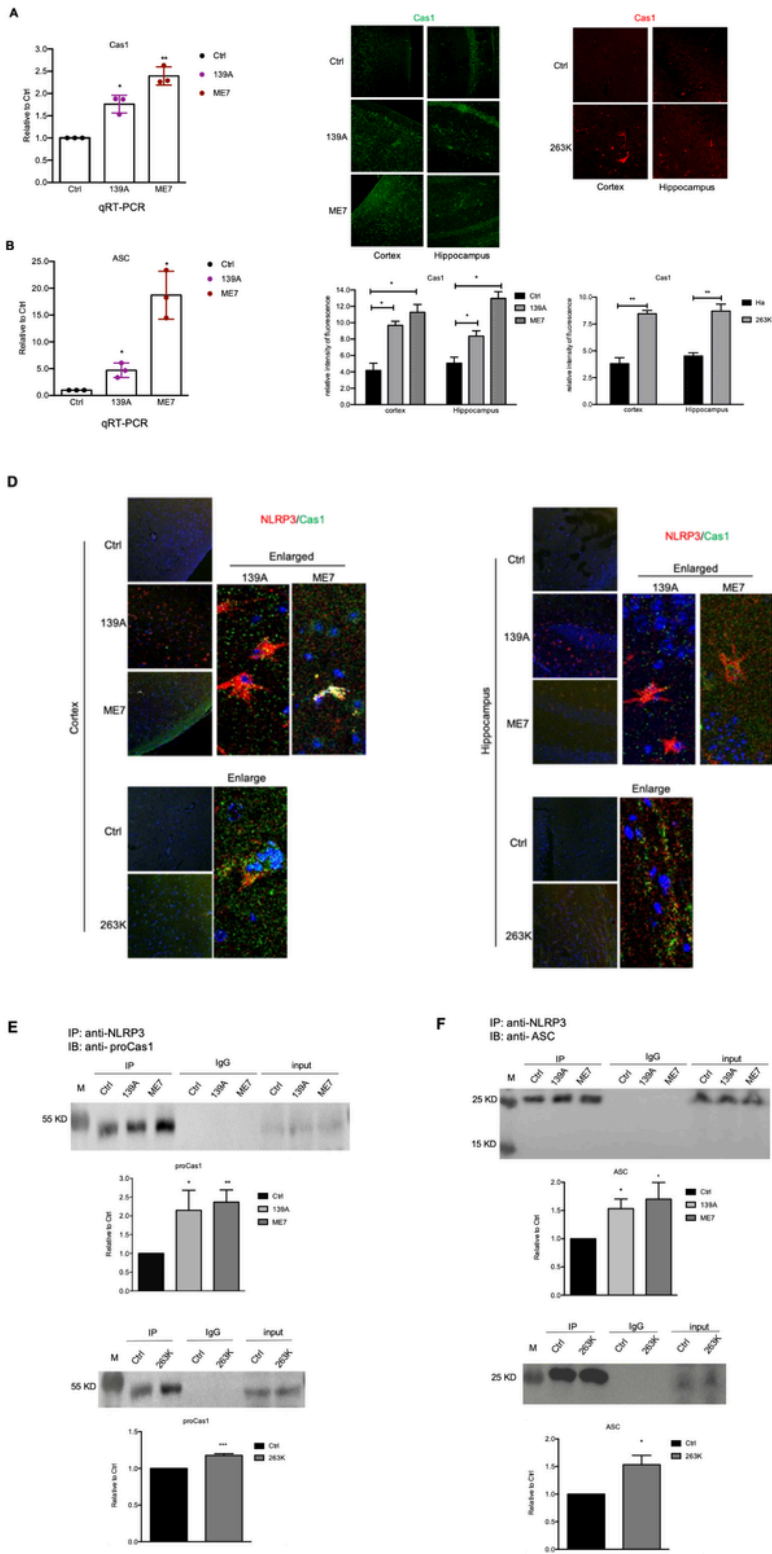
Figure 3

Analyses of brain Caspase-1 and ASC in the prion infected rodent models at terminal stage. **A.**Caspase-1 specific qRT-PCR of the brain RNAs of 139A- or ME7-infected mice and the age-matched mice. **B.** ASC specific qRT-PCR of the brain RNAs of 139A- or ME7-infected mice and the age-matched mice. Relative fold changes of Caspase-1 or ASC mRNAs are marked on Y-axis. Graphical data denote mean + SD (n=3). **C.** Representative images of Caspase-1 specific IFAs of the brain sections of scrapie agents 139A-

and ME7-infected mice (*left*) and 263K-infected hamsters (*right*). Relative fluorescent intensities of NLRP3 signals in the brain slices of prion infected animals compared to the individual controls (n=3) are showed on the bottom. **D.** Representative merged images of double stained IFAs with anti-NLRP3 (*red*) and anti-Caspase-1 (*green*) in the brain sections of the prion infected rodent models. Brain regions of cortex and hippocampus are indicated on the left. The enlarged images of prion infected animals are showed on the right each graph. Upper panels: 139A- and ME7-infected mice. Bottom panels: 263K-infected hamsters. **E.** IP assays of the brain homogenates of the prion infected rodent models using anti-NLPR3 as capturing antibody and anti-Caspase-1 as blotting antibody. **F.** IP assays of the brain homogenates of the prion infected rodent models using anti-NLPR3 as capturing antibody and anti-ASC as blotting antibody. IgG: isotopic mouse IgG. Input: an aliquot of brain homogenates directly loaded into SDS-PAGE as control. The relative gray values of the precipitated Caspase-1 and ASC bands after normalized with the individual β-actin (n=3) are marked below each graph.
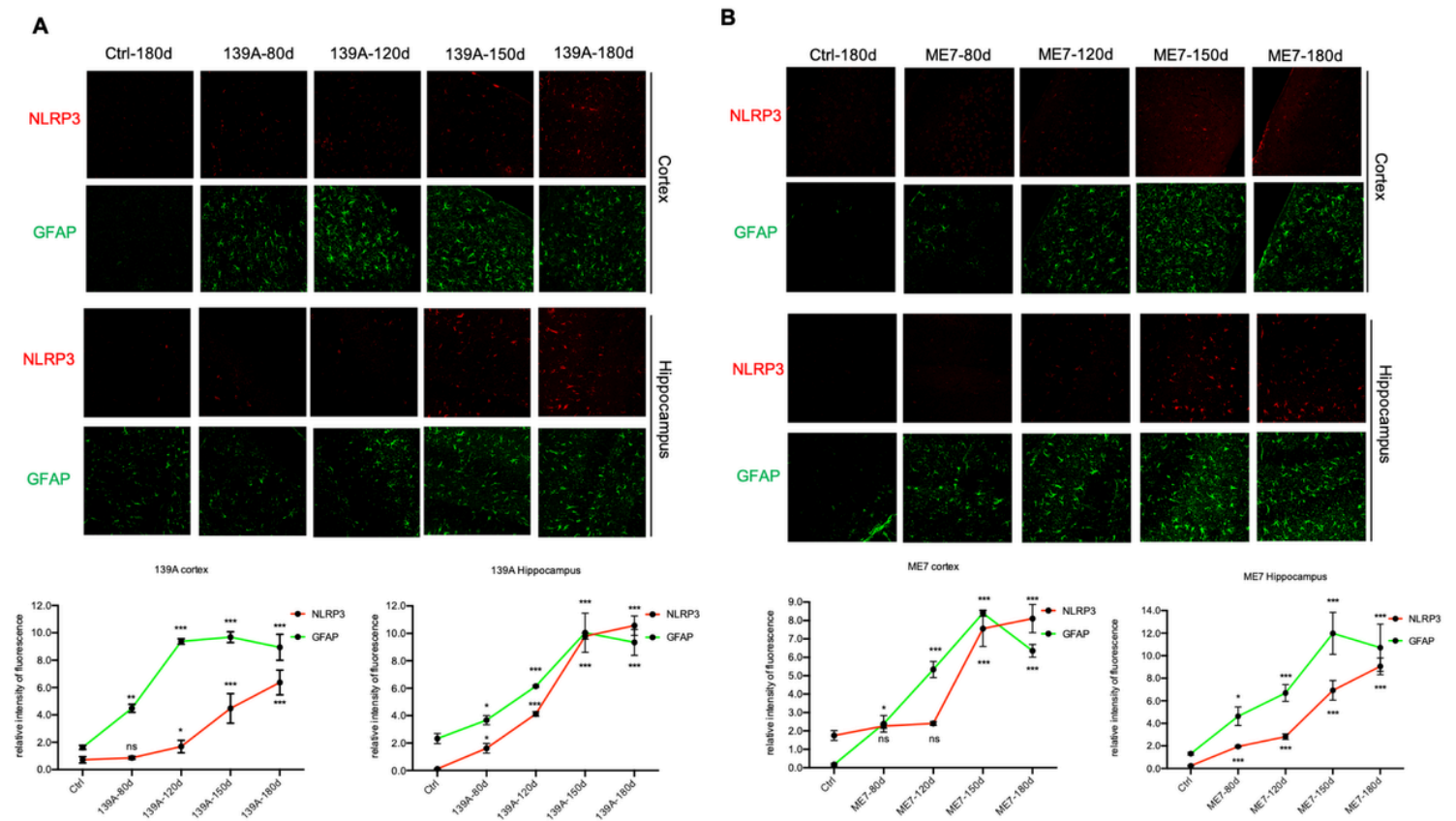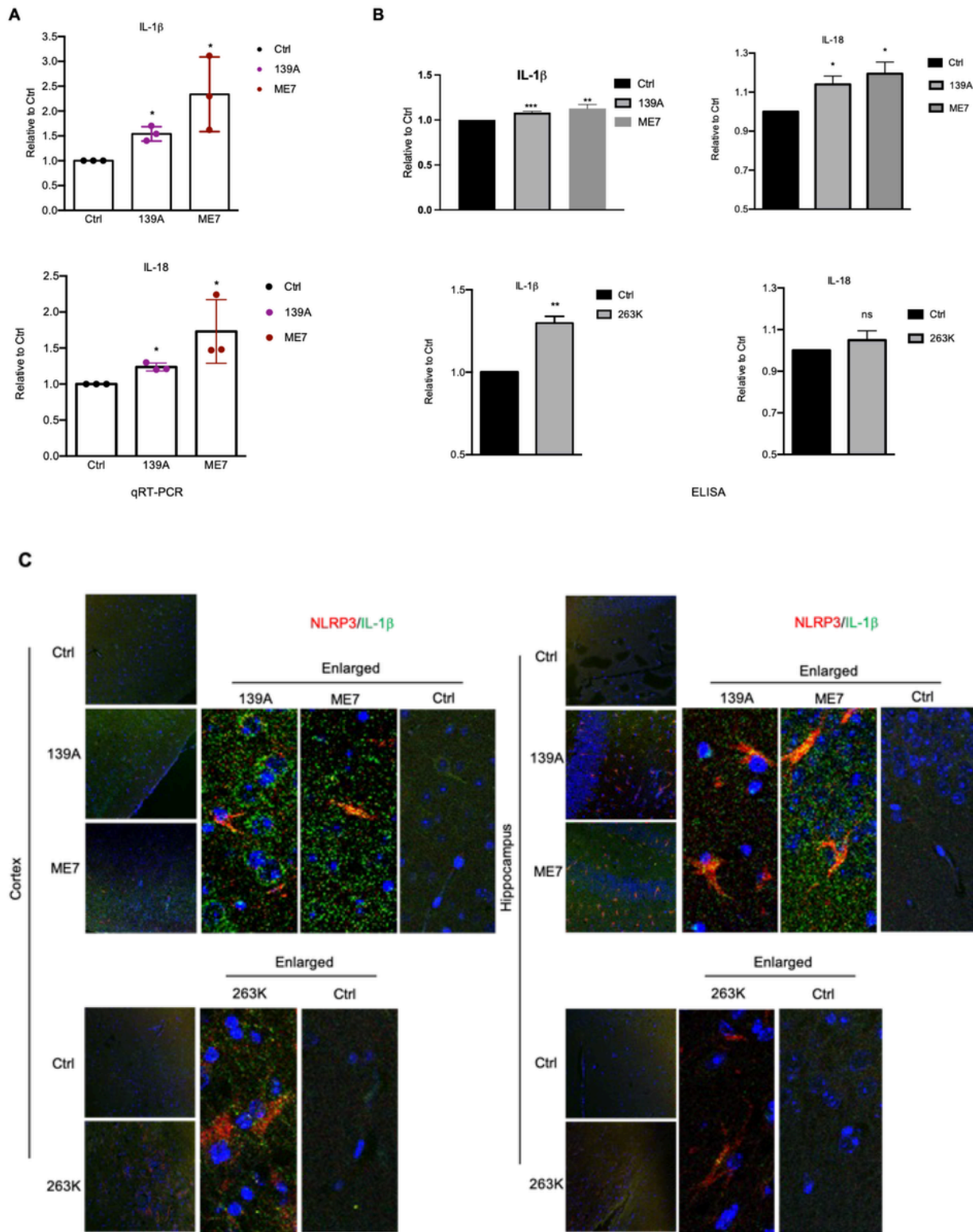

Figure 4

NLPR3 and GFAP specific IFAs of the brain sections of prion infected mice collected at different time-points post-inoculation. A. Representative images of 139A-infected mice. **B.** Representative images of ME7-infected mice. The brain sections of the infected mice collected at 80- 120- 150- and 180- (terminal stage) dpi are indicated above the images. Brain regions of cortex and hippocampus are indicated on the left. Relative fluorescent intensities of NLRP3 (*red*) and GFAP (*green*) in the brain regions of the infected mice compared to the normal control are showed below the graphs.

Figure 5

Analyses of brain IL-1band IL-18 in the prion infected rodent models at terminal stage. **A.** IL-1band IL-18 specific qRT-PCRs of the brain RNAs of 139A- or ME7-infected mice and the age-matched mice. Relative fold changes of IL-1b(upper) and IL-18 (lower) mRNAs are marked on Y-axis. Graphical data denote mean + SD (n=3). **B.** ELISA for IL-1b and IL-18 in the brain homogenates. Upper panel: 139A- and ME7- infected mice controlled with normal mice. Low panel: 263K-infected hamsters controlled with normal

hamsters. **C.** Representative merged images of double stained IFAs with anti-NLRP3 (*red*) and anti- IL-1b(*green*). Brain regions of cortex and hippocampus are indicated on the left. The enlarged images are showed on the right each graph. Upper panels: 139A- and ME7-infected mice. Bottom panels: 263K-infected hamsters.
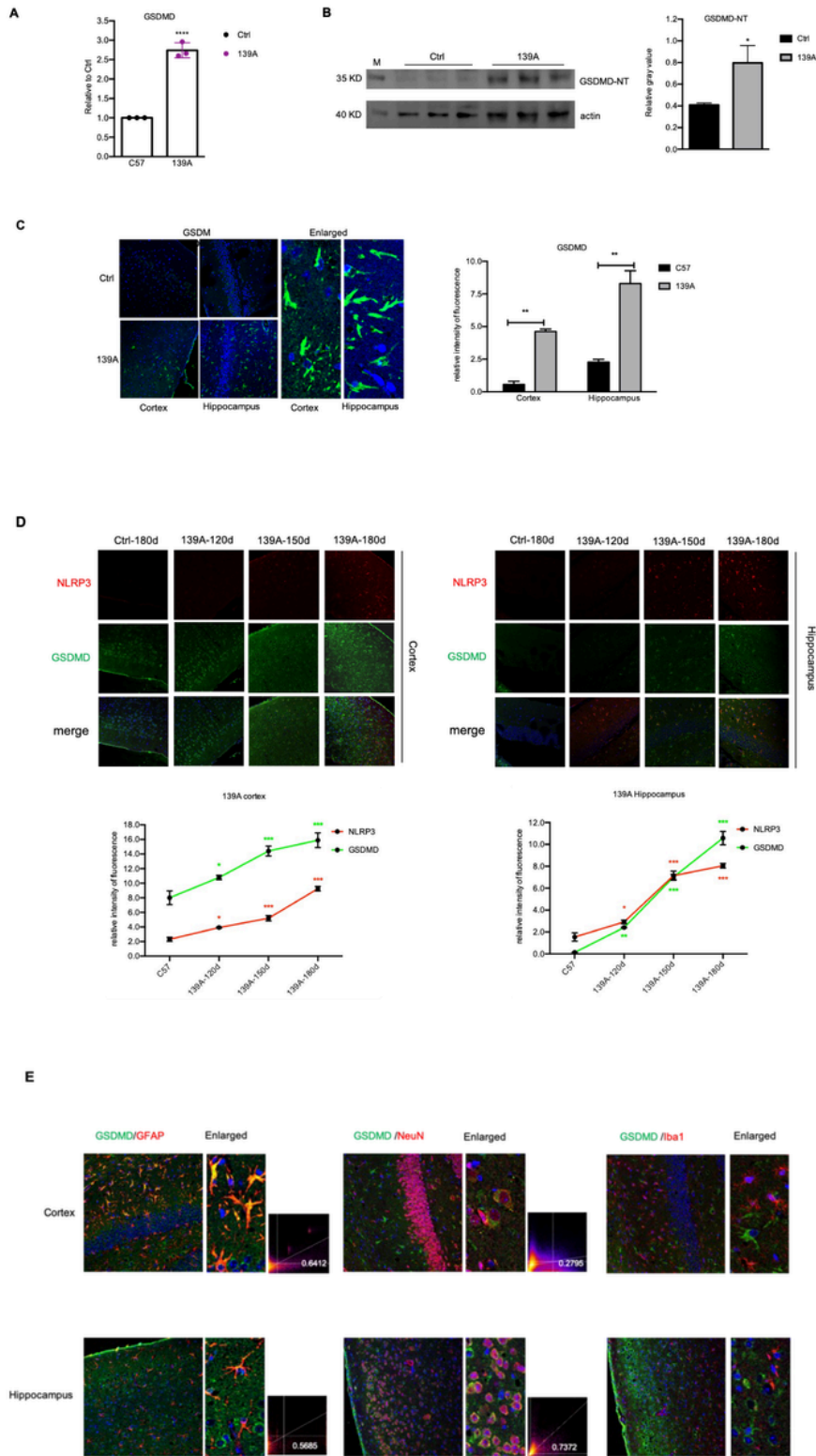

Figure 6

Analyses of brain GSDMD in the prion infected rodent models. **A.** GSDMD specific qRT-PCR assays of the brain RNAs of 139A-infected mice at terminal stage. Relative fold changes of GSDMD mRNAs in the infected mice normalized with the data of control are marked on Y-axis. **B.** GSDMD-NT specific Western blot of brain homogenates of 139A-infected mice at terminal stage. The relative gray values of GSDMD-NT normalized with the individual β-actin (n=3) are marked on the right. **C.** Western blot Representative images of GSDMD-specific IFAs of the brain sections from 139A-infected mice at terminal stage and normal control. The enlarged images of 139A-infected mice are showed on the right of the graphs. Relative fluorescent intensities of GSDMD signals in the brain slices of 139A-infected mice compared to the normal control (n=3) are showed on the right. **D.** Representative images of double stained IFAs with anti-GSDMD (*green*) and anti-NLPR3 (*red*) of the brain slices from 139A-infected mice collected at different times post-inoculation. Relative fluorescent intensities of NLRP3 (*red*) and GFAP (*green*) in the brain regions of the infected mice compared to the normal control are showed below the graphs. **E.** Representative images of double stained IFAs by anti-GSDMD (*green*) together with anti-GFAP, anti-NeuN or anti-Iba1 (*red*) of the brain sections from 139A-infected mice at terminal stage.